Hydrol. Earth Syst. Sci. Discuss., 6, 6007–6033, 2009
www.hydrol-earth-syst-sci-discuss.net/6/6007/2009/

Hydrology and Earth System Sciences Discussions

Papers published in *Hydrology and Earth System Sciences Discussions* are under open-access review for the journal *Hydrology and Earth System Sciences*

Buffering of the salinity intrusion in estuaries by channel convergence

P. S. Gay and J. O'Donnell

University of Connecticut, Department of Marine Sciences, 1080 Shennecossett Road, Groton, CT 06340, USA

Received: 11 August 2009 – Accepted: 31 August 2009 – Published: 22 September 2009

Correspondence to: P. S. Gay (peter.gay@uconn.edu)

Published by Copernicus Publications on behalf of the European Geosciences Union.

Abstract

A one-dimensional advective-diffusive model is used to investigate the influence of channel convergence on the runoff-dependence of the distance salt intrudes from the ocean into estuaries. We express the runoff dependence of the dispersion coefficient as $K \sim \rho^{\beta}$, and that of the intrusion extent as $x_s \sim \rho^{-\gamma}$, where ρ is the normalized freshwater discharge into the estuary, and show that $\beta+\gamma=1$ for a prismatic channel. For a channel that is narrower at the river end we find that for relatively low runoff, $\beta+\gamma<1$. Using two decades of salinity observations in the Chesapeake Bay, and Delaware Bay and a shorter data-set for the Connecticut River, we show that channel convergence may contribute significantly to buffering the salinity intrusion. We demonstrate that in a well-mixed estuary with significant convergence, the geometry alone can explain the relatively weak response of the salt intrusion to fluctuations in river discharge. In contrast, a less tapered, but more stratified estuary dominated by gravitational circulation will respond more strongly to runoff fluctuations.

1 Introduction

The proximity of fresh water and convenient access to the ocean has led to the development of many cities along estuaries near the limit of the intrusion of salt from the ocean. The location of the transition from fresh to saline water is critical to the design of intakes for municipal water systems. As river flow control infrastructure for irrigation projects has expanded, regulations have been developed to protect drinking water and salt sensitive ecosystems (Jassby et al., 1995) from being polluted by ocean water. Dredging projects to deepen navigation channels as well as land reclamation projects have also been regulated for this reason (Sanders and Piasecki, 2002).

These practical considerations have resulted in a few long records of measurements of salinity and river discharge and a considerable literature on the relationship between tidal mixing, runoff and the distribution of salt in estuaries. Analytical models of in-

HESSD

6, 6007–6033, 2009

creasing complexity have been developed to understand the salinity distribution, from tidal prism models (Ketchum, 1951) and one-dimensional advective-diffusive models (Cameron and Pritchard, 1963) through two-dimensional models (Hansen and Rattray, 1965 – hereafter denoted HR65; Chatwin, 1976; Lung and O'Conner, 1984) that combine the dynamics of buoyancy driven exchange flow and tidal mixing with salt-conservation.

Assuming a uniform salinity gradient, as in the central regime of HR65, for a uniform (prismatic) channel in steady state, the magnitude of the buoyancy driven circulation is predicted to vary as the 1/3 power of the runoff and the salinity intrusion is expected to vary as the negative 1/3 power of the runoff (Monismith et al., 2002). Ralston et al. (2007) and Lerczak et al. (2008) find that during periods of low flow in the lower Hudson River (which has negligible channel convergence), the intrusion distance varies as expected. However, during high discharge periods, the variation is less than predicted. The environmental impact of the salinity intrusion during low runoff (and high tide) is of greatest concern and in regions which experience a Spring freshet or episodic rainfall, low runoff conditions will prevail throughout most of the year.

Other models of salt transport in estuaries have led to slightly different conclusions regarding the runoff dependence of the salinity intrusion and the related runoff dependence of the dispersion coefficient, which in a one-dimensional model accounts for all processes which result in the up-stream transport of salt. Scaling the results of HR65 or Chatwin (1976) leads to the conclusion that the dispersion coefficient should vary as the 2/3 power of the runoff (Monismith et al., 2002; Lerczak et al., 2008), provided this coefficient is treated as spatially uniform. We derive this relation using the steady-state advective-diffusive equation for a prismatic channel by assuming the dispersion coefficient varies as the square of the salinity gradient (Prandle, 1981; Monismith et al., 2002; Lerczak et al., 2008). Savenije (1993b) developed an expression, which he found to be successful at modeling the salinity intrusion in alluvial estuaries, which relates the dispersion coefficient to the square root of the runoff. This leads, for prismatic channels, to the conclusion that the intrusion length should vary as the inverse root of the runoff.

HESSD

6, 6007–6033, 2009

However their dispersion coefficient (see Savenije, 2005) is expressed as proportional to the subtidal axial velocity, or the runoff divided by the cross-sectional area, so that if the runoff all enters at the head of the estuary and the channel convergence is linear, the dispersion coefficient has a logarithmic dependence on cross-sectional area. In either case, the runoff dependence of the dispersion coefficient is considerably stronger than for a well-mixed, tidally-dominated estuary in which dispersion is expected to be only weakly dependent on the runoff.

Garvine et al. (1992) reported a much weaker than expected runoff-dependence of the salinity intrusion in the Delaware Bay (DB), a tidally dominated estuary which may be expected to have relatively runoff-independent dispersion and a relatively large variability of the intrusion length, and proposed that "a powerful buffering agent" must be active. They suggested the cause may be a feedback between stratification and circulation (see Park and Kuo, 1996). Ralston et al. (2008) expanded on this idea and parameterized the vertical mixing as dependent on the bottom boundary layer thickness assuming that straining of the axial salinity gradient by the tides balances turbulent mixing at the top of the bottom boundary layer. When the boundary layer thickness is less than the water depth, the vertical mixing scale is reduced so that horizontal flux due to the exchange flow increases. Inclusion of stratification-dependent mixing through use of the bottom boundary layer thickness reduces the runoff dependence of the salinity intrusion (Lerczak et al., 2008). Ralston et al. (2008) note that both the axial salinity gradient and the Richardson number increase with runoff, decreasing the boundary layer thickness and vertical mixing while increasing the gravitational circulation. This correlation between increased runoff and decreased mixing damps the response of the salt intrusion to variations in discharge.

However, it is well established that the channel geometry also influences how far up-estuary salt intrudes (Savenije, 1993b; Lewis and Uncles, 2003; MacCready, 2004; Brockway et al., 2006). Whitney and Garvine (2006) suggest that "buffering" due to channel convergence can account for the "weak dependence between estuarine salinity and river discharge". Savenije (1993a) finds the intrusion length to be more sensitive

to runoff when the channel taper is weak. Monismith et al. (2002) observed in the San Francisco Bay estuary that the salinity intrusion varied as the inverse 1/7 power of the runoff. Using a numerical simulation of the San Francisco Bay estuary with a constant vertical mixing coefficient to study the influence of non-uniform bathymetry on the salinity intrusion, they found that the intrusion varied inversely with the 1/5 power of the runoff. Ralston et al. (2008) conclude that "spatial variability in depth and cross-sectional area have a much greater impact on response of the system to changes in discharge than effects of stratification on vertical mixing." They note that the increase in cross section as salt is pushed seaward offsets the increase in velocity that would otherwise result from increased runoff.

For high runoff conditions when stratification is increased and, in extreme cases, the salt may be forced out of the estuary entirely, the behavior is expected to be considerably different from times of low or moderate runoff (MacCready et al., 2002; Lerzcak et al., 2008). For a sudden, large change in runoff, the response timescale of the salinity intrusion complicates analysis (Savenije, 2006; MacCready, 2008; Ralston et al., 2008). Estuaries are more likely to be in equilibrium, steady state during high runoff due to reduced response time (Lerczak et al., 2008) but then they exhibit greater response to tidal and spring-neap variability (Ralston et al., 2008) so that it is more difficult to measure their subtidal mean state.

In this paper we use a steady one-dimensional advective-diffusive salt budget model for a linearly tapered estuarine channel with uniform salinity gradient to demonstrate the influence of a uniform variation in channel cross-section on the relationship between the runoff-dependencies of the salinity intrusion and the dispersion coefficient. Since depth typically varies little compared to width in many coastal-plain estuaries (Savenije, 2005), this is almost equivalent to a linearly varying width. Though depth variations have a much stronger influence on dispersion than width variations (Ralston et al., 2008), depth rarely varies in a uniform manner either along or across the estuary. Savenije (1993a) notes that an exponentially-tapered estuary will result in unaltered tidal range and excursion along the estuary so that tidal dispersion is a constant

HESSD
6, 6007–6033, 2009

along the estuary for given runoff. However, lateral increases in depth are often found near the mouths of estuaries (ebb and flood channels are common) and Coriolis effects can become significant as the estuary width increases. While parameterizations of the dispersion coefficient variation with channel geometry and tidal amplitudes have been developed, the complicated geometry of real estuaries and the difficulty of making estimates of this coefficient has limited the empirical evidence for these models. Since there is little compelling evidence for variable dispersion coefficients and since we are interested in demonstrating the integrated effect of cross-sectional area variations on the salinity intrusion over the entire length of the estuary, we use a spatially uniform dispersion coefficient. This is consistent with the approach used by Garvine (1992) and Monismith et al. (2002) and related earlier studies of transport in estuaries.

In the following section we summarize the data from the Chesapeake Bay (CB), the Delaware Bay (DB) and the Connecticut River (CR) used to test the model results.

The details of the model are presented in Sect. 3. This is followed by a descriptive summary of the observations in Sect. 4 which graphically compares the salinity intrusion variation with runoff using long time-series of observations for the CB, DB and a shorter record from CR. These observations are compared with the model-predicted runoff dependence of the salinity intrusion using parameters estimated from the bathymetry of each estuary. For reference, the influence of channel taper on the runoff-dependencies of the salinity intrusion is illustrated for a HR65-like estuary in which dispersion is expected to vary as the 2/3-power of the runoff, and for tidally-dominated estuaries in which the dispersion is expected to be independent of the tidally-averaged runoff. We summarize the paper and results in Sect. 5.

2 Data

The salinity data used for CB and DB, as well as runoff and bathymetry data, are discussed in Gay and O'Donnell (2008), in addition to the method used to estimate total runoff based on gauged input to the main rivers. All bathymetry data are from the

HESSD
6, 6007–6033, 2009

National Oceanic and Atmospheric Administration. For CB, over 21 locations along the axis of the bay were sampled by the Chesapeake Bay Program's Mainstem Water Quality Monitoring Program throughout the water depth between 0 and 3 times a month since 1984. We have used data from 1984 through 2002 and averaged these vertically over the water column at each station and over each month. Runoff data are available from the United States Geological Service (USGS) for seven main rivers entering CB and a factor of 1.43 is applied to their sum to represent ungauged regions of the watershed and the difference between precipitation and evaporation.

The data for DB, collected by the Delaware River Basin Commission, cover the same time-span as those for CB but are only surface measurements and the coverage for the 12 axial stations is more sparse, with significant temporal gaps. Stratification is sufficiently weak in DB that surface measurements should be adequately representative of the average over the depth (Garvine et al., 1992). Note however that this approximation is likely to be least good at times of high runoff and during neap ebb tide (Whitney and Garvine, 2006). The principal source of runoff is the Delaware River measured by the USGS at Trenton, N.J., and following Garvine et al. (1992), a factor of $(0.52)^{-1}$ is applied to account for net discharge into DB which is not measured at this gauge (see also Whitney and Garvine, 2006).

Salinity data for CR were collected during the late 1990s (Howard-Strobel et al., 1997). These were sampled throughout the water column and averaged over the depth. Estimation of the uncertainties as the standard deviation in binning the data is not possible due to the paucity of data. The runoff in CR is measured at Thompsonville, CT, at USGS station 01184000, and is multiplied by a factor of 1.2 to account for ungauged runoff seaward of this station (see Gay and O'Donnell, 2008).

Figure 1 shows the cross-sectional area for CB, DB and CR and the range of the observed 2 psu and 5 psu isohalines for CB and DB (data are binned according to runoff) and the 2 psu isohalines for CR (not binned). The monthly positions of the isohaline are evaluated using a linear interpolation between stations whose monthly mean vertically-averaged (or surface in the case of DB) salinities bracket the salinity

HESSD
6, 6007–6033, 2009

defining the intrusion.

An approximation for a linearly tapered channel representing CB and DB is detailed in Gay and O'Donnell (2008). Here we use channel tapers of 1.0 m^2/m for CB and 2.0 m^2/m for DB, and channel lengths of 300 km and 150 km, respectively, where we take the channel length as being equal to the cross-sectional area at the mouth (0.3 km^2 for both CB and DB) divided by the channel convergence rate. These model channel geometries are depicted in Fig. 1. We have not included the tributaries in CB and as a result our model channel is, perhaps, too narrow but these are merely scale estimates. In Sect. 4 we investigate the influence of increasing the model channel dimensions of CB within plausible limits. For CR, we estimate from the data shown in Fig. 1 a length of 60 km and a taper of 0.05 m^2/m so that the cross-sectional area at the mouth is 0.003 km^2. Note that while the estuary length exceeds the salinity intrusion length, it plays no role in the analysis in this paper. The bathymetry of CB, DB, and CR is shown in Fig. 1.

3 Model development

Here we develop a simple model to examine the influence of linear variation of cross-sectional area on the runoff-dependence of the salinity intrusion. We do not explicitly address independent variations in width and depth. In many estuaries the laterally averaged depth does not vary much in the along-channel direction (Savenije, 2005). We acknowledge that unresolved bathymetric variations may influence the relative importance of baroclinic exchange and determine the effective dispersion coefficient and its runoff dependence, however for the reasons we outline at the end of the Introduction, we assume the dispersion coefficient is uniform throughout the tapered channel. Gay and O'Donnell (2007) demonstrate that both the dispersion coefficient and the salinity gradient are likely to depend on variation in channel cross-section and that a change of channel convergence is required to reverse the curvature of the salinity profile from negative at the mouth to positive at the up-estuary reaches of the salinity intrusion. The

HESSD
6, 6007–6033, 2009

axial gradient of the depth-averaged salinity is here assumed to be uniform as in the central regime of HR65. We demonstrate below that in order to have a linear variation in salinity along the estuary, either the dispersion coefficient or the cross-sectional area must vary linearly, and the other must then be a constant.

Defining a coordinate system with x measured up-estuary from the mouth, or high salinity end of the estuary, the axially integrated one-dimensional steady-state advective-diffusive equation with no sources or sinks can be expressed as

$$-\frac{KA(x)}{R} = \frac{s(x)}{\mathrm{d}s/\mathrm{d}x}, \quad (1)$$

where K is the axial dispersion coefficient (Hunkins, 1981; Jay et al., 1997; Savenije, 2005), $A(x)$ is the cross-sectional area, and R is the runoff, assumed to enter up-estuary of the salinity intrusion. It is clear that if $s(x)$ is to be a linear function of x so that $\mathrm{d}s/\mathrm{d}x$ is a constant, since R is also assumed to be spatially uniform due to the river entering at the head of the estuary, then $KA(x)$ must have a linear dependence on x so that either K or A must depend linearly on x but not both. Also note that differentiating Eq. (1) leads to $K\frac{\mathrm{d}A}{\mathrm{d}x}=-R$ (see Whitney and Garvine, 2006), so that the equation is not valid in the limit of zero channel converence, i.e., for uniform channels. On the other hand this equation does imply that for linear channel convergence, K should be a constant which lends support to our approach.

We assume the axial depth- and width-averaged salinity gradient $\mathrm{d}s/\mathrm{d}x$ is uniform from the mouth of the estuary to the up-estuary limits of the salinity intrusion, and replace $\mathrm{d}s/\mathrm{d}x$ in Eq. (1) by $(s_{x_s}-s_0)/x_s$ where s_{x_s} is the salinity used to define the salinity intrusion, x_s, and s_0 is the salinity at the mouth, assumed constant with respect to changes in R. Expressing the cross-sectional area as $A=A_0-ax$, where A_0 is the mean-tide cross-sectional area at the mouth and a is the decrease in cross-sectional area with axial distance (see Fig. 2), Eq. (1) then becomes

$$\frac{K(A_0 - ax)}{R} = \frac{x_s}{\sigma}, \quad (2)$$

HESSD
6, 6007–6033, 2009

where we have defined $\sigma \equiv (s_0 - s_{x_s})/s(x) = -x_s \frac{ds/dx}{s(x)}$ so that if there is a similarity relation $ds/dx \propto s(x)$ then $\frac{x_s}{\sigma}$ is a constant. The analysis used here remains valid so long as $\frac{\partial x_{s_0}}{\partial t} \ll \frac{\partial x_s}{\partial t}$, i.e., the isohaline typically observed at the estuary mouth should move little relative to the isohaline defining the salinity intrusion so that it can be used as the reference point for this approximation to the salinity gradient.

The asymptotic approach to the salinity of waters external to the mouth usually occurs somewhat seaward of the mouth, especially during coastal upwelling conditions or offshore winds, so that the region of negative curvature of the salinity profile does not extend very far into the estuary (Gay and O'Donnell, 2008). The validity of the linear gradient approximation is also improved by taking s_{x_s} large enough that it is not in the higher curvature region at the up-estuary end of the salinity profile. However, to be a practical measure of the extent of the salinity intrusion, it is desirable to have $s_{x_s} \ll s_0$. Note that in an estuary like CB, the regions of strong gradient occur only near the mouth and the head, while the central reach has fairly uniform salinity (Gay and O'Donnell, 2008; Austin, 2004). In this case, the uniform salinity gradient as applied in our model represents a mean salinity gradient over the length of the estuary.

Evaluating A and s at x_s and solving Eq. (2) for x_s gives

$$x_s = \frac{A_0}{a}\left(1 + \frac{R}{\sigma K a}\right)^{-1} . \quad (3)$$

For $\sigma K a \ll R$, Eq. (3) reduces to Eq. (1) and the runoff behavior of x_s is determined by the behavior of K, A_0 and R. $\frac{K A_0}{R}$ is the "salinity-intrusion length" (Zimmerman, 1988) for a uniform channel with cross-sectional area equal to A_0. If, on the other hand, $\sigma K a \gg R$, then x_s is constant and independent of runoff. This limit shows that channel convergence buffers fluctuations in x_s resulting from fluctuations in river discharge, assuming K and σ are independent of a. Of course, in a given estuary if the channel convergence is changed, it is likely that K would also change, but to first order we assume we can investigate the influence of small variations in a treating K as con-

stant. The term $\frac{Ka}{R}$ is equal to the salinity intrusion length scale, $\frac{KA_0}{R}$, divided by the convergence length scale, $\frac{A_0}{a}$, and vanishes as the convergence length approaches infinity.

Savenije's "dispersion reduction rate" differs from our $\frac{R}{Ka}$ by being multiplied by the inverse of Van den Burgh's factor (Savenije, 2005), $k \equiv \frac{A}{R} \mathrm{d}K/\mathrm{d}x$. Assuming that we can use the linear convergence length in place of the exponential length-scale, Savenije's relation (Eq. 5.48 in Savenije, 2005) can be expressed as $x_s = \frac{A_0}{a} \ln\left(1+\frac{1}{k}\frac{Ka}{R}\right)$. Noting that $\lim_{x\to 0}\left[\ln(1+x)-(1+\frac{1}{x})\right] = 0$, this is identical with Eq. (3) for $\sigma Ka \ll R$ so long as we replace σ with $\frac{1}{k}$. These are conditions of high (mean) runoff, low dispersion, and weak channel convergence. Using the steady advective-dispersion relation, Eq. (1), Van den Burgh's constant expresses a similarity relation between $\frac{\mathrm{d}s/\mathrm{d}x}{s}$ and $\frac{\mathrm{d}K/\mathrm{d}x}{K}$, so that we can write $k = \frac{x_s}{\sigma}\frac{\mathrm{d}K/\mathrm{d}x}{K}$ with $\frac{x_s}{\sigma}$ constant.

The intrusion length, x_s, is plotted in Fig. 3 as a function of a and $\frac{R}{K}$ for $A_0 = 3\times10^5$ m^2, $s_0 = 30$, and $s_{x_s} = 2$. Clearly the sensitivity of the intrusion to variation in R is reduced as the convergence increases, though this seems to be a relatively weak effect. The intrusion length increases with decreases in either the runoff or the convergence rate, or increased dispersion.

To develop a power law dependence of the salt intrusion on runoff, we express the intrusion length and dispersion coefficient as $x_s \equiv C_1 R^{-\gamma}$ and $K \equiv C_2 R^{\beta}$, respectively, where $\gamma \geq 0$, $\beta \geq 0$, $C_1 > 0$, and $C_2 > 0$. It is important to recognize that the values of γ and β for a particular estuary are determined by the interactions of physical processes and the details of the geometry. Alternative parameterizations of the runoff dependence are possible. However, several studies have used this power-law form and estimated C_1 and γ from observations, obtaining a wide range of values. We can demonstrate that for a prismatic channel, the HR65 model dynamics imply $\beta = 2/3$ by assuming that the salinity structure is self-similar, $s \propto \mathrm{d}s/\mathrm{d}x$, so that $K \sim (-\mathrm{d}s/\mathrm{d}x)^k$ (see Prandle, 1981). Equation (1) then implies $(-\mathrm{d}s/\mathrm{d}x)^{k+1} A_0 = R s_0$ or $-\mathrm{d}s/\mathrm{d}x \sim R^{1/(k+1)}$ so that with $k = 2$

(see Monismith et al., 2002; Lerczak et al., 2008) we get $K \sim R^{2/3}$. Recall that $ds/dx<0$ with our coordinate definitions.

We define $B=\frac{-\partial x_s}{\partial R}$ as the geometric buffering factor. With this definition, B is positive and decreasing values represent decreased response of the salinity intrusion length to runoff changes. We now consider how B varies with γ. Note that $\frac{\partial x_s}{\partial R} \leq 0$ and that $B=\frac{\gamma}{R} x_s$. If $\frac{\partial B}{\partial \gamma}>0$, then for a decrease in γ, the intrusion length is more buffered and less sensitive to runoff variations. When $C_1 \neq C_1(\gamma)$, there is a value of $\gamma=\gamma_{\max}$ below which $\frac{\partial B}{\partial \gamma}>0$ but above which $\frac{\partial B}{\partial \gamma}<0$. Since $\frac{\partial B}{\partial \gamma}=\frac{C_1}{R^{\gamma+1}}[1+\gamma(\frac{1}{C_1}\frac{\partial C_1}{\partial \gamma}-\log(R))]$, assuming $C_1 \neq C_1(\gamma)$ implies that $\frac{\partial B}{\partial \gamma}>0$ for $\gamma<\gamma_{\max}=\frac{1}{\log(R)}$. However, this result suffers from dimensional inconsistency.

If instead we use $x_s \equiv C_3 \rho^{-\gamma}$ and $K \equiv C_4 \rho^{\beta}$ in Eq. (3), we get

$$\gamma = \frac{\log(\frac{C_3<R>}{\sigma A_0 C_4}) + \log(\rho^{1-\beta} + \frac{a\sigma C_4}{<R>})}{\log(\rho)} . \quad (4)$$

For zero convergence, $a=0$, we can satisfy $\beta+\gamma=1$ by setting $\sigma A_0 C_4 = <R> C_3$ so that

$$\gamma = \frac{\log(\rho^{1-\beta} + aC_3/A_0)}{\log(\rho)} . \quad (5)$$

This choice of C_4 makes sense if we express the intrusion length as $x_s = <x_s> \rho^{-\gamma}$ where $<x_s>$ is the long-term mean salinity intrusion, so that $C_3 = <x_s>$ and $C_4 = \frac{<R><x_s>}{\sigma A_0} = <K>$ since Eq. (1) applies in the mean.

In order to evaluate γ for a given β, we need an estimate of C_3. One possibility is to fit C_3 and γ to observations as is done in the following section. In order to investigate graphically the characteristics of Eq. (4), we estimate C_3 as $<x_s>$ and use the observed mean salinity intrusion length in CB and in DB. We again take $A_0=3\times10^5\,\mathrm{m}^2$, $s_0=30$, and $s_{x_s}=2$ and plot $\beta+\gamma$ in Fig. 4 for $0<\rho<1$ and $0<a<2$. Figure 4a, c are for $<x_s>=78$ km as in DB, while Fig. 4b, d are for $<x_s>=270$ km as in CB. In Fig. 4a, b,

we set β=0, while in Fig. 4c, d, β=2/3. In Fig. 4a, b, with β=0, the contours therefore show values of γ and demonstrate that for low runoff, the salinity intrusion is increasingly buffered as the convergence increases. For a longer mean intrusion length, $<x_s>$=270 km as in CB, Fig. 4b, d show that a weaker convergence results in positive values of γ. As the runoff increases toward long-term mean values, smaller convergence rates are required for γ>0, but we do not consider the model to be applicable near ρ=1. In Fig. 4c, d, γ becomes negative when the contours $\beta+\gamma<2/3$. We conclude that for the model to be useful in estuaries in which $\beta\sim2/3$, the channel convergence parameter, a, must be small so that we can have $\gamma\geq0$.

4 Applications

In order to investigate the applicability of this model in real estuaries, archived salinity observations are used to evaluate the monthly averaged salinity intrusion distance for CB, DB, and CR. These data are binned according to runoff and the runoff dependence is compared with predictions from the prismatic channel theory (i.e., $\beta+\gamma$=1) and from Eq. (5). These observations are not synoptic and this likely results in some error due to aliasing. Figures 5–7 show observations of salinity intrusion to the 2 psu isohaline as a function of runoff for CB, DB, and CR, respectively. The error bars represent the standard deviation in discharge-rate bins. The more limited data set available for CR does not allow for binning of the data so standard deviations do not appear in Fig. 7. Lines showing a runoff-dependence of the salinity intrusion with γ=1/7, γ=1/3, and γ=1 are plotted in these figures. To compare with the prediction of γ given by Eq. (4) for β=0 or β=2/3 in each estuary, we use a least-squares procedure to fit γ and C_3 to the observations by writing $x_s \equiv C_3\rho^{-\gamma}$ as $\log(x_s)=\log(C_3)-\gamma\log(\rho)$. This value of C_3 is then used in Eq. (5) to estimate γ for a given value of β. In fitting γ and C_3 to the observations, it turns out that C_3 is very close to the mean observed salinity intrusion length, $<x_s>$.

For the 2 psu isohaline in CB (Fig. 5), a linear regression to the logarithm of

HESSD
6, 6007–6033, 2009

the observed x_s gives a runoff dependence of the salinity intrusion of $\gamma \approx 0.012$ and $C_3 = 269 \times 10^3$. C_3 is essentially the same as the mean of the observations of the 2 psu salinity intrusion length in CB, which is 270 km. Note that this is not much less than our model convergence length of 300 km. The mean runoff is $<R> = 2{,}145\ m^3/s$. With $a = 1.0\ m^2/m$ and $A_0 = 0.3\ km^2$, we must have $\beta < -1.01$ to have $\gamma_{\rho=0.3} > 0.012$, where the subscript indicates that γ is evaluated at $\rho = 0.3$. A negative value of β does not seem plausible as we expect the dispersion to increase with an increase in runoff due to the increase in buoyancy-driven exchange.

Since our geometric model of CB does not include the tributaries, and since the cross-sectional area varies greatly near the mouth (Fig. 1), we next investigate whether reasonable modifications to the representation of the geometry (the channel convergence, a, and the cross-sectional area at the mouth, A_0) allow the model Eq. (4) to yield estimates of γ that are consistent with observations. With $\beta = 2/3$ and the convergence reduced to $a = 0.353\ m^2/m$, we get $\gamma_{\rho=0.3} = 0.012$. We get equivalent results if the cross-sectional area at the mouth is increased to $A_0 = 0.850\ km^2$ and note that both modifications of the model geometry give a convergence length-scale of 850 km. With $\beta = 0$, if the convergence is reduced to $a = 0.765\ m^2/m$ or if the cross-sectional area at the mouth is increased to $A_0 = 0.392\ km^2$, we get $\gamma_{\rho=0.3} = 0.012$. The convergence length-scale of 392 km required for $\beta = 0$ to give observed values of γ is much closer to the 300 km which we determined from Fig. 1 than the 850 km required for $\beta = 2/3$. We conclude that for low runoff, $\beta = 0$ is a better model for CB than $\beta = 2/3$ when channel convergence is taken into account using Eq. (4), at least when the runoff is 0.3 of the mean. This would imply that CB behaves as a well-mixed estuary under these conditions.

For the 2 psu isohaline in DB (Fig. 6), with a mean runoff of $R = 761\ m^3/s$, the logarithm of the observations are best fit by a line with slope $\gamma \approx 0.17$ and $C_3 = 74 \times 10^3$. C_3 is slightly lower than the observed mean intrusion length, 78 km and half our model convergence length of 150 km. Applying Eq. (5) for $a = 2.0\ m^2/m$ and $A_0 = 0.3\ km^2$, a value of $\beta = 0.062$ gives $\gamma_{\rho=0.3} = 0.17$, matching the observations. This would suggest that

HESSD
6, 6007–6033, 2009

DB also behaves as a well-mixed estuary at relatively low runoff when channel convergence is taken into account using Eq. (4).

For the 2 psu isohaline in CR (Fig. 7), with the mouth taken where CR enters LIS and s_0 taken as the long-term mean salinity in eastern LIS (28 psu), $\gamma \approx 0.34$ best fits the observations, a much larger magnitude of variation than in CB and DB and very close to the 1/3 value predicted for a prismatic-channel HR65-like estuary. $C_3 = 7.6 \times 10^3$ is significantly lower than the observed mean salinity intrusion length, 9.1 km and much lower than our model geometrical convergence length of 60 km. The mean runoff is $R = 468\,m^3/s$. Taking $a = 0.05\,m^2/m$ and $A_0 = 0.003\,km^2$, a value of $\beta = 0.62$ gives $\gamma = 0.34$. Thus it would appear that CR behaves closer to the predictions for the variability of dispersion for a prismatic HR65-like estuary ($\beta = 2/3$) than either CB or DB under conditions of low runoff.

5 Discussion and conclusions

In this study we have developed a simple model of the salinity intrusion in an estuary which converges toward the river end at a constant rate using an advective-diffusive salt balance. To achieve a simple analytic result, and for comparison with results of Garvine (1992) and Monismith et al. (2002), we approximate both the axial salinity gradient and the dispersion coefficient as being spatially uniform. The goal is to describe the influence of a tapering cross-section on the runoff-dependence of the salinity intrusion and its relation to the runoff dependence of the dispersion coefficient. It is expected that channel convergence would result in buffering the salinity intrusion against fluctuations in river discharge as compared with a prismatic, non-tapered, channel because the isohaline will move to a region of different cross-sectional area. Increased cross-sectional area, when runoff increases and the isohaline tends to move seaward, allows increased exchange of salt which opposes the seaward advance of the intrusion. Similarly, if runoff decreases and the isohaline moves up-estuary, it encounters smaller cross-sections which decreases the exchange of salt. In addition, the decreas-

ing volume per unit axial length means that the reduced runoff will fill a smaller volume, slowing the advance of the intrusion.

The model, Eq. (5), expresses the salinity intrusion distance as $x_s \equiv C_3 \rho^{-\gamma}$ and the dispersion coefficient as $K \equiv C_4 \rho^{\beta}$ so that we may compare results with other studies that have used a power-dependence on runoff. In order to satisfy $\beta+\gamma=1$ for zero channel convergence, $a=0$, so that when $\beta=2/3$ we will have $\gamma=1/3$, we require $\sigma A_0 C_4 = <R> C_3$. We can then use least-squares to fit γ and C_3 to observations. We found this model to be useful for the points we are demonstrating, but only for conditions of relatively low runoff and weak channel convergence. However, the latter condition is typical of estuaries and the former is of greatest concern for the environmental impact of the salinity intrusion and also likely to be typical in regions where runoff is episodic or occurs predominantly during a Spring freshet.

We find that as dispersion becomes increasingly runoff-dependent, the salinity intrusion becomes less runoff-dependent and we described the dependencies of this relationship on channel geometry and runoff levels. This analysis helps to understand how a well-mixed estuary with constant dispersion may show weaker than expected variability in the salinity intrusion, as in DB and CB, which have significant convergence, and a more stratified estuary may be less buffered than expected as in CR which has negligible convergence. CR appears to behave like a classic prismatic-channel HR65-like estuary with $\beta=2/3$ giving a value of $\gamma \sim 1/3$, very close to that which is observed.

It is clear from Fig. 1 and the results of this study that channel geometry and the extent of the salinity intrusion varies widely between estuaries. Many studies have sought to provide a relatively simple model which can be used to predict the salinity intrusion. A uniform dispersion coefficient and a prismatic, non-converging channel was investigated by early researchers and led to the observation by Garvine (1992) and Monismith (2002) that the intrusion typically varied much more weakly than predicted by these models. We have shown that channel convergence can help to explain these observations, with the acknowledgement that more sophisticated parameterizations of channel geometry and the dispersion coefficient, and ultimately more detailed

approaches such as numerical modeling, are required to accurately predict the salinity intrusion in estuaries.

6 Notation

A: cross-sectional area

A_0: cross-sectional area at seaward boundary

a: change of cross-sectional area with axial distance (channel convergence)

B: buffering factor, B=$\frac{-\partial x_s}{\partial R}$

C_1, C_3: coefficients for parameterization of salinity intrusion

C_2, C_4: coefficients for parameterization of dispersion coefficient

k: Van den Burgh constant

K: axial dispersion coefficient

K_{tide}: dispersion coefficient for runoff-independent dispersion

R: runoff entering up-estuary of the salinity intrusion

s: cross-section average salt concentration

s_{x_s}: salinity defining the intrusion length

s_0: salinity at the seaward end of the estuary

x: axial coordinate measured up-estuary from the seaward end

x_s: intrusion length to a given isohaline, s

β: runoff-dependence of the dispersion coefficient

γ: inverse runoff-dependence of the salinity intrusion length

$\gamma_{\max}$: value of γ for minimum buffering

ρ: non-dimensional runoff-parameter

σ: $(s_0 - s_{x_s})/s(x)$

HESSD
6, 6007–6033, 2009

Acknowledgements. We acknowledge financial support through the National Oceanographic Partnership Program-funded FRONT project (N00014-99-1-1020) and the National Oceanic and Atmospheric Administration-funded LISICOS program (NA04NOS4730256). We thank Professor R. W. Garvine of the University of Delaware for generously providing data he acquired in the Delaware Bay.

References

Brockway, R., Bowers, D., Hoguane, A., Dove, V., and Vassele, V.: A note on salt intrusion in funnel-shaped estuaries: Application to the Incomati estuary, Mozambique, Estuar. Coast. Shelf S., 66, 1–5, 2006.

Cameron, W. M. and Pritchard, D. W.: Estuaries, in: The Sea: Ideas and Observations on Progress in the Study of the Seas, Vol. 2, The Composition of Sea-Water, Comparative and Descriptive Oceanography, edited by: Hill, M. N., John Wiley and Sons, New York, 306–324, 1963.

Chatwin, P. C.: Some remarks on the maintenance of the salinity distribution in estuaries, Estuar. Coast. Mar. Sci., 4, 555–566, 1976

Garvine, R. W., McCarthy, R. K., and Wong, K. C.: The axial salinity distribution in the Delaware estuary and its weak response to river discharge, Estuar. Coast. Shelf S., 35, 157–165, 1992.

Gay, P. S. and O'Donnell, J.: Comparison of the salinity structure of the Chesapeake Bay, the Delaware Bay and Long Island Sound using a linearly tapered advection-dispersion model, Estuar. Coasts, V32, 68–87, doi:10.1007/s12237-008-9101-4, 2008.

Gay, P. S. and O'Donnell, J.: A simple advection-dispersion model for the salt distribution in linearly tapered estuaries, J. Geophys. Res., 112, C07021, doi:10.1029/2006JC003840, 2007.

Hansen, D. V. and Rattray, M.: Gravitational circulation in straits and estuaries, J. Mar. Res., 23, 104–122, 1965.

Howard-Strobel, M. M., O'Donnell, J., Bohlen, W. F., and Cohen, D. R.: Observations on the hydrography of the Connecticut River during high and low river discharges, Proceedings of the 3rd Biennial Long Island Sound Research Conference, University of Connecticut, Avery Point, 16 October 1996, 1997.

Jassby, A. D., Kimmerer, W. J., Monismith, S. G., Armor, C., Cloern, J. E., Powell, T. M.,

Schubel, J. R., and Vendlinksi, T. J.: Isohaline position as a habitat indicator for estuarine populations, Ecol. Appl., 5(1), 272–289, 1995.
Lerczak, J. A., Geyer, W. R., and Ralston, D. K.: The temporal response of the length of a partially-stratified estuary to changes in river flow and tidal amplitude, J. Phys. Oceanogr., 39(4), 915–933, doi:10.1175/2008JPO3933.1, 2008.
Lerczak, J. A. and Geyer, W. R.: Modeling the lateral circulation in straight, stratified estuaries, J. Phys. Oceanogr., 34(6), 1410–1428, 2004.
Lewis, R. E. and Uncles, R. J.: Factors affecting longitudinal dispersion in estuaries of different scale, Ocean Dynam., 53, 197–207, 2003.
Lung, W. S. and O'Conner, D. J.: Two-dimensional mass transport in estuaries, J. Hydraul. Eng., 110(10), 1340–1357, 1984.
MacCready, P.: Toward a unified theory of tidally-averaged estuarine salinity structure, Estuaries, 27(4), 561–570, 2004.
MacCready, P. M., Hetland, R. D., and Geyer, W. R.: Long-term isohaline salt balance in an estuary, Cont. Shelf Res., 22, 15912–16001, 2002.
Monismith, S. G., Kimmerer, W., Burau, J. R., and Stacey, M. T.: Structure and flow-induced variability of the subtidal salinity field in northern San Francisco Bay, J. Phys. Oceanogr., 32, 3003–3019, 2002.
Park, K. and Kuo, A. Y.: Effect of Variation in Vertical Mixing on Residual Circulation in Narrow, Weakly Nonlinear Estuaries, in: Buoyancy Effects on Coastal and Estuarine Dynamics, edited by: Aubrey, D. G. and Friedrichs, C. T., Coastal and Estuarine Studies 53, AGU, 301–317, 1996.
Ralston, D. K., Geyer, W. R., and Lerczak, J. A.: Subtidal salinity and velocity in the Hudson River estuary: Observations and modeling, J. Phys. Oceanogr., 38(4), 753–770, 2008.
Sanders, B. F. and Piasecki, M.: Mitigation of salinity intrusion in well-mixed estuaries by optimization of freshwater diversion rates, J. Hydraulic Eng., 128(1), 64–77, 2002.
Savenije, H. H. G.: Comment on "A note on salt intrusion in funnel-shaped estuaries: Application to the Incomati estuary, Mozambique" by Brockway et al. (2006), Estuar. Coast. Shelf S., 68, 703–706, 2006.
Savenije, H. H. G.: Salinity and Tides in Alluvial Estuaries, Elsevier BV, 194 pp., Amsterdam, 2005.
Savenije, H. H. G.: Composition and driving mechanisms of longitudinal tidal average salinity dispersion in estuaries, J. Hydrol., 144, 129–141, 1993a.

Savenije, H. H. G.: Predictive model for salt intrusion in estuaries, J. Hydrol., 148, 203–218, 1993b.

Valle-Levinson, A., Reyes, C., and Sanay, R.: Effects of bathymetry, friction, and rotation on estuary-ocean exchange, J. Phys. Oceanogr., 33, 2375–2393, 2003.

Whitney, M. M. and Garvine, R. W.: Simulating the Delaware Bay buoyant outflow: Comparison with observations, J. Phys. Oceanogr., 36, 3–21, 2006.

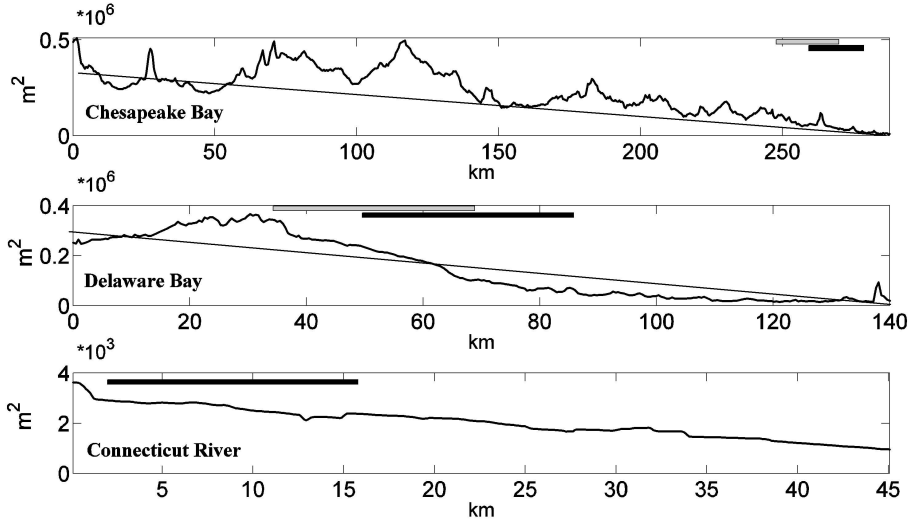

Fig. 1. Cross-sectional area for Chesapeake Bay (upper plot), Delaware Bay and River (center plot) and the Connecticut River (lower plot). The straight lines depict the model geometry for Chesapeake Bay and Delaware Bay. Also shown are the range of observations of salinity intrusion to the 2 psu (black horizontal bars) and 5 psu (gray horizontal bars) isohalines. For the Connecticut River, only the 2 psu observations are shown. For the Delaware Bay and the Chesapeake Bay, observations of salinity intrusion are binned by runoff levels.

HESSD
6, 6007–6033, 2009

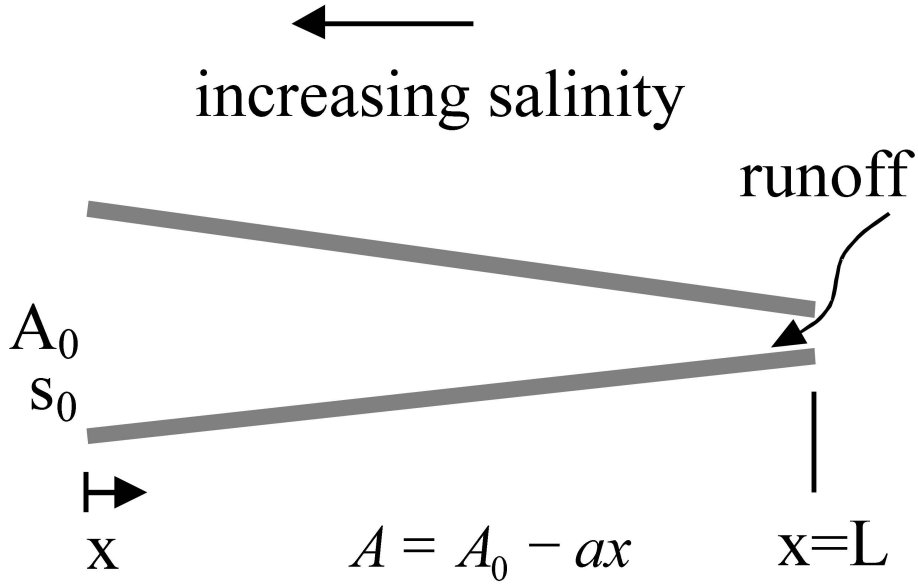

Fig. 2. Definitions of parameters and variables involved in the one-dimensional steady-state model of an estuarine segment. The ocean is to the left while the low-salinity end is to the right. The segment is of length L which we define in this paper as the convergence length, A_0/a. Thick gray lines indicate variation of cross-sectional area ($A=A_0-ax$) with axial distance and may be due to either varying depth or varying width or both. A_0 is the cross-sectional area at the seaward end and a is the channel taper or convergence. The salinity, s, is averaged over the cross-section. Runoff is evaluated as gauged runoff in principal rivers entering the segment multiplied by a factor to account for ungauged runoff, ignoring precipitation and evaporation. All the runoff into a segment is taken as entering upstream of the salinity intrusion.

HESSD
6, 6007–6033, 2009

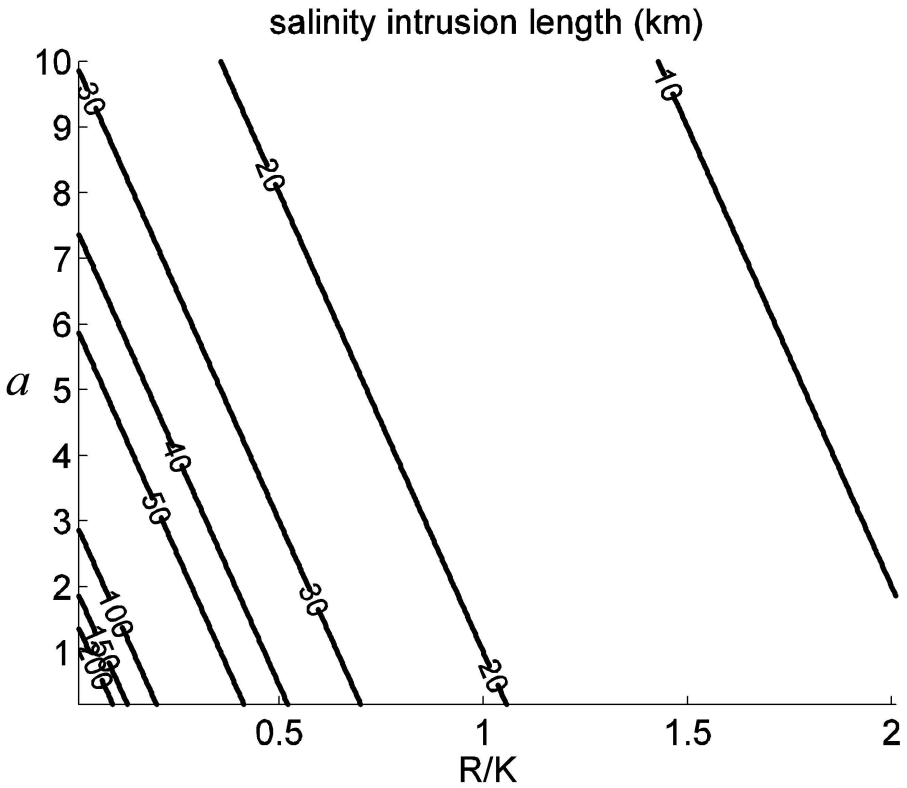

Fig. 3. Salinity intrusion length in an estuary using Eq. (3) as a function of channel convergence, a (m^2/m), and the ratio of the runoff and the dispersion coefficient, R/K, for $s_{x_s}/s_0=2/30$ and $A_0=3\times10^5$ m^2.

HESSD
6, 6007–6033, 2009

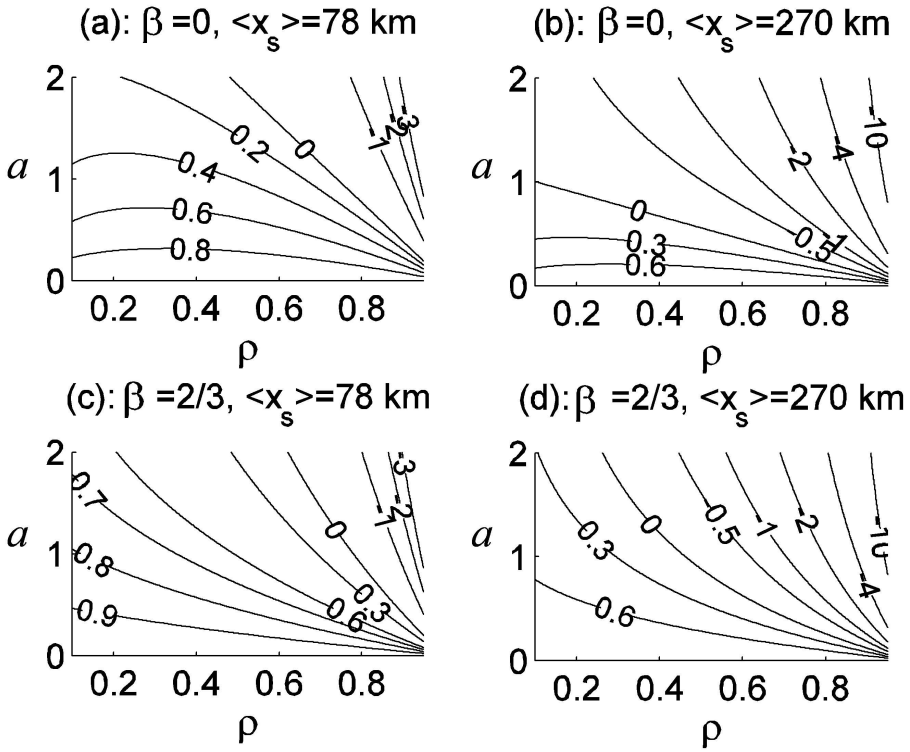

Fig. 4. The sum, $\beta+\gamma$, of the exponents expressing runoff dependence of the axial dispersion and salinity intrusion length predicted by Eq. (4) as a function of channel convergence, a (m^2/m), and normalized runoff, $\rho=R/<R>$. **(a)** shows contours of $\beta+\gamma$ for $\beta=0$ and $C_3=78$ km. Note that for $\beta=0$, these contours are equivalent to contours of γ. **(b–d)** show $\beta+\gamma$ for ($\beta=0$, $C_3=270$ km), ($\beta=2/3$, $C_3=78$ km), and ($\beta=2/3$, $C_3=270$ km), respectively. The salinity intrusion is defined by $\frac{s_x}{s_0}=\frac{2}{30}$.

HESSD
6, 6007–6033, 2009

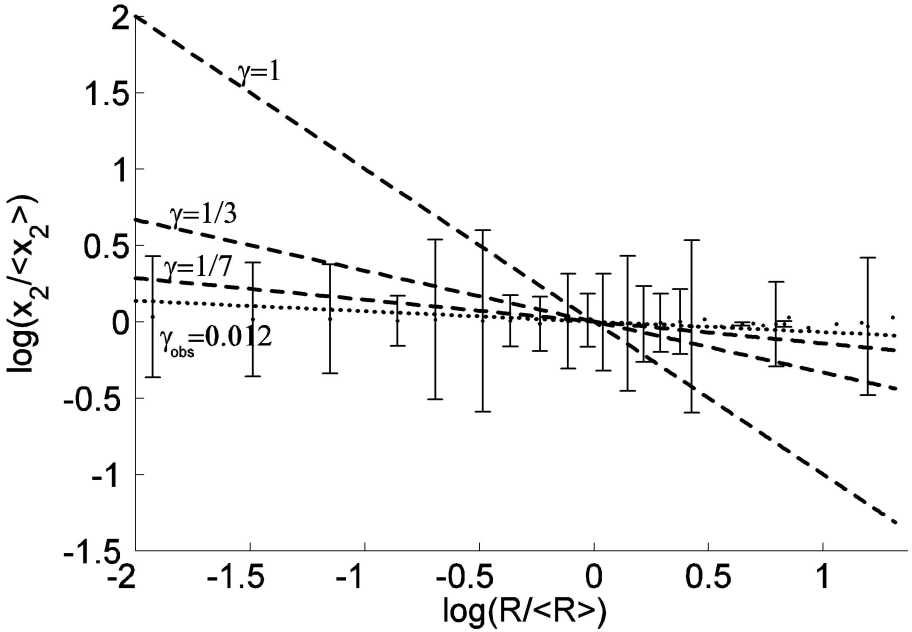

Fig. 5. Intrusion of the cross-section average 2 psu isohaline in the Chesapeake Bay as a function of runoff. Dots and errorbars represent binned averages and their standard deviations. Dotted line shows the best fit to the observations. Dashed lines are for $\gamma=1/7$, $\gamma=1/3$, and $\gamma=1$.

HESSD
6, 6007–6033, 2009

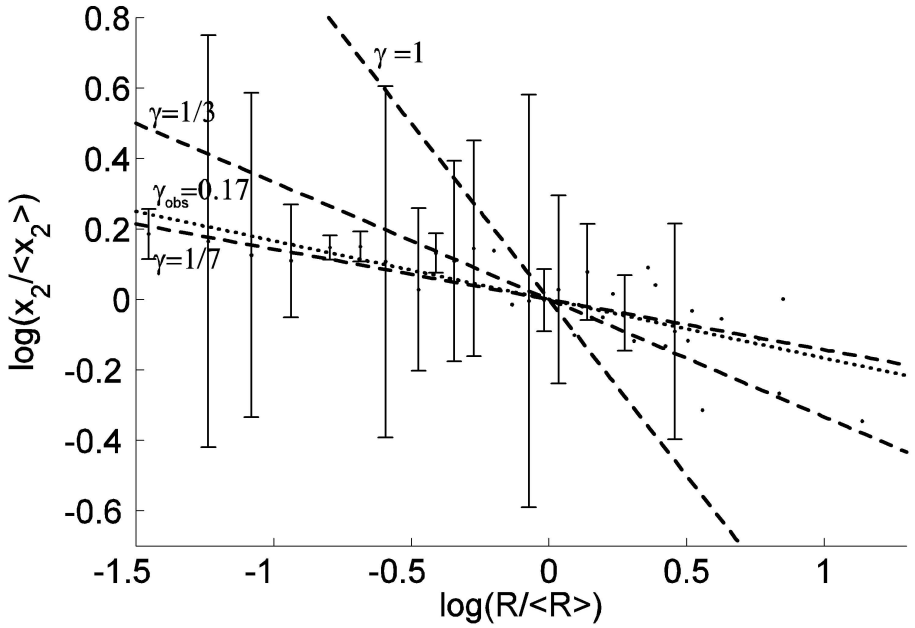

Fig. 6. Intrusion of the cross-section average 2 psu isohaline in the Delaware Bay as a function of runoff. Dots and errorbars represent binned averages and their standard deviations. Dotted line shows the best fit to the observations. Dashed lines are for $\gamma=1/7$, $\gamma=1/3$, and $\gamma=1$.

HESSD
6, 6007–6033, 2009

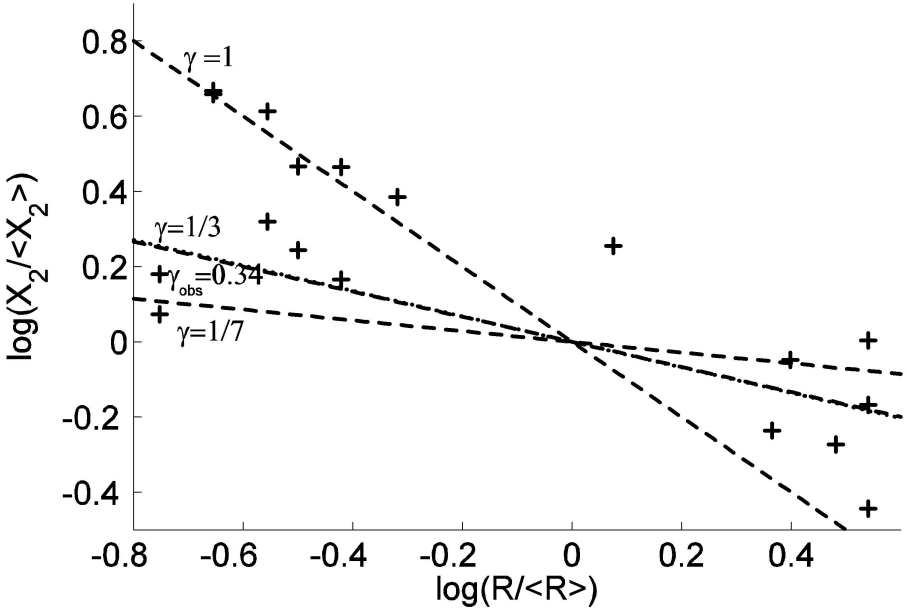

Fig. 7. Intrusion of the cross-section average 2 psu isohaline in the Connecticut River as a function of runoff. Dashed lines are for γ=1/7, γ=1/3, and γ=1. The dotted line (best fit to the observations) is indistinguishable from the γ=1/3 line.

HESSD
6, 6007–6033, 2009